ARCHIVES OF ELECTRICAL ENGINEERING VOL. 73(4), pp. 977–997 (2024)

DOI 10.24425/aee.2024.152106

State-of-charge estimation based on improved back-propagation neural network for lithium-ion batteries in energy storage power stations

XIAOHONG ZHU✉, MINGWAN ZHUANG, WEIRONG YANG, XIUQUAN LI, HANG DAI

Qujing Power Supply Bureau, Yunnan Power Grid Co. Ltd.,
Cuifeng East Road, Qilin District, Qujing City, Yunnan Province, China
e-mail: {✉ 13769887755/13988977711/13577351166}@163.com, 532822995@qq.com, daihang132@foxmail.com

(Received: 26.03.2024, revised: 16.11.2024)

Abstract: This paper develops a novel approach for the state of charge (SOC) estimation of Lithium-ion batteries in energy storage power stations, leveraging an improved back-propagation (BP) neural network optimized by an immune genetic algorithm (IGA). Addressing the paramount importance of accurate SOC estimation for enhancing battery management systems, this work proposes a methodological enhancement aimed at refining estimation precision and operational efficiency. First, the mechanisms of temperature, current, and voltage impacts on SOC are revealed, which serve as the inputs of the neural network. Second, the improved BP neural network's structure and optimization through an IGA are designed, emphasizing the mitigation of traditional BP neural networks' limitations including slow convergence speed and complex parameterization. Through an extensive experimental setup, the proposed model is validated against standard BP neural networks across various discharge experiments at different temperatures and discharge currents. Results prove that the estimation accuracy of the proposed method reaches as high as 98.15% and faster converges compared to the traditional BP network, thereby being valuable practically.

Key words: back-propagation neural network, energy storage, immune genetic algorithm, lithium-ion battery, state of charge

1. Introduction

To address the energy crisis and environmental pollution caused by fossil fuels, renewable energy generation, represented by wind and solar power, has rapidly developed, with its generation capacity continually increasing [1, 2]. According to a study report by the Rocky Mountain

Institute (RMI), by 2030, wind and solar projects are expected to account for over one-third of global electricity [3]. However, renewable energy generation faces challenges of intermittency and variability, which cannot meet the high-quality electricity demands of the grid and end-users [4]. In this context, efficient regulation of renewable energy generation becomes significantly important. Large-scale battery storage stations, which can regulate grid peak load and frequency and effectively ensure electricity quality, have seen rapid development [5, 6]. As illustrated in Fig. 1, the commonly-used large-scale storage stations' battery packs are typically composed of many lithium-ion battery cells connected in series and parallel [7]. During manufacturing and use, lithium-ion batteries can exhibit variations in parameters such as self-discharge rate, internal resistance, voltage, and capacity. These differences manifest as capacity or voltage inconsistencies among series-connected cells in a battery pack when fully charged or discharged, leading to overcharging or over-discharging in some modules. Over-discharging occurs when the battery voltage is too low, enhancing the pack's heterogeneity and creating a vicious cycle of increased likelihood of overcharging and discharging in subsequent uses. Additionally, overheating issues during charging and discharging can lead to premature failure or even danger. The effective management of lithium-ion batteries is crucial for enhancing the safety and lifespan of both the batteries and the storage station [8–10].

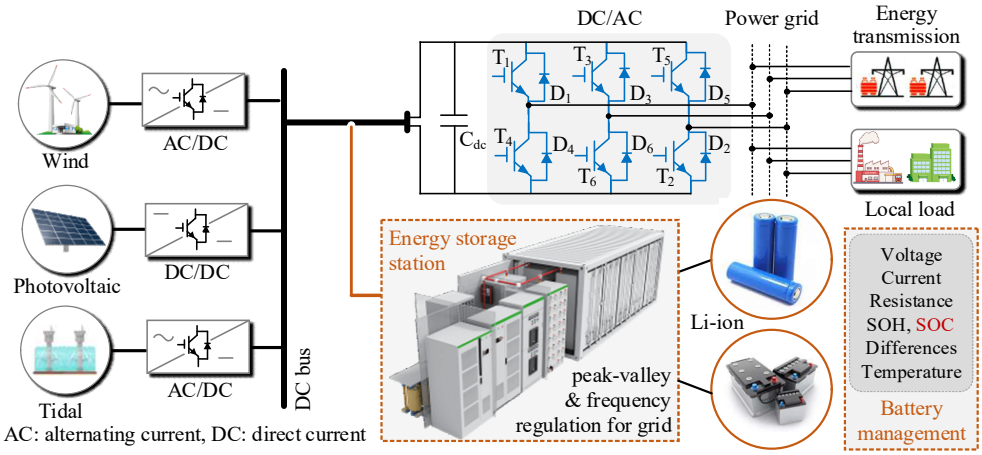

Fig. 1. Battery arrays in battery arrays in energy storage stations connected with grid

The primary functions of a lithium-ion battery management system in a storage station include controlling charging and discharging, measuring parameters like voltage, current, and temperature, balancing among cells, estimating battery state of charge (SOC) and state of health (SOH), and diagnosing faults in the battery pack [11]. Accurate SOC estimation, which represents the degree of battery charging and discharging, can prevent excessive charging and discharging, thereby increasing battery lifespan and reducing costs [12, 13]. Thus, accurate SOC estimation for lithium-ion batteries in storage stations is a current hot topic.

The commonly-used methods for lithium-ion battery SOC estimation include the voltage method, discharge test method, ampere-hour integration method, internal resistance method, fuzzy logic method, and neural network method [14].

1. The voltage method relies on the known relationship between battery voltage and SOC to estimate the SOC value by detecting the output voltage of the battery. It is simple and easy to operate, but when the SOC of lithium-ion batteries is between 20% and 90%, the battery voltage changes within a small range, thus requiring precise voltage measurements, which places high demands on hardware [15].
2. The discharge test method involves discharging the battery at a constant current, and the product of discharge time and current represents the remaining battery capacity. While commonly used in laboratories, this method is less suitable for energy storage stations due to the need for continuous measurements over long periods [16, 17].
3. The ampere-hour integration method requires to continuously measure the current flow, calculates the power consumption of the battery using integration, and then subtracts the initial SOC value to obtain the actual SOC. However, the introduction of integration calculations can lead to integration errors [18].
4. The internal resistance method relies on the relationship between SOC and internal resistance [19]. Accurate measurement and analysis of the internal impedance of the battery are necessary, but the internal resistance varies continuously during battery operation, making it difficult to measure precisely and thus challenging to estimate SOC using this method [20].
5. The fuzzy logic algorithms mimic human thinking patterns through fuzzy reasoning. They have the advantage of being versatile and not relying on precise battery mathematical models. However, accurate cost functions and fuzzy relationships must be designed; otherwise, the estimation accuracy may be low [21].
6. Neural networks can learn the internal laws of nonlinear systems through sample data learning. Neural networks can approximate arbitrary complex nonlinear mappings with arbitrary precision, thus enabling the establishment of neural networks for highly nonlinear systems such as batteries to estimate SOC [22–24]. The advantage of neural network methods is that they do not rely on precise battery models, are convenient, fast, and have high accuracy. Among these methods, neural network methods have obvious advantages in terms of estimation accuracy and thus deserve further research.

Neural networks used for battery SOC estimation include back-propagation (BP) neural networks, recurrent neural networks (RNNs), convolutional neural networks (CNNs), and long short-term memory (LSTM) networks, and so on [25, 26]. These neural network (NN) methods are capable of capturing temporal dependencies and spatial features within battery data, thus providing more accurate and reliable SOC estimates. Among these neural networks, BP neural networks excel in their versatility and high adaptability [27]. However, they also have the disadvantages of slow convergence speed and high complexity in parameter design, which may affect the estimation accuracy [28]. Currently, through algorithm optimization and appropriate network design, it is possible to effectively mitigate these shortcomings of BP neural networks, enabling them to perform powerful functions in the field of battery SOC estimation. In addition to the neural networks used in SOC estimation, there are many advanced neural networks in the other fields. Paper [29] presents a sophisticated approach to time series forecasting, emphasizing the importance of accurate predictions in energy management. In [30], the use of deep learning is explored for enhancing the reliability of state estimations in complex heating systems. Literature [31] investigates reinforcement learning strategies in financial trading, highlighting the potential for improved decision-making in low-reward scenarios. Paper [32] addresses the critical need for

reliable verification methods in neural network applications, ensuring model robustness and accuracy. Additionally, literature [33] showcases the use of optimized learning algorithms to enhance predictive maintenance in automotive engineering. Paper [34] delves into the precision of neural network approximations, pushing the boundaries of computational accuracy. Finally, [35] illustrates the potential of hybrid neural networks in financial forecasting, combining the strengths of different neural architectures to improve predictive performance. These studies underscore the versatility and power of neural networks in addressing diverse and complex real-world problems.

This paper proposes a method that utilizes immune genetic algorithms (IGAs) to optimize BP neural networks, addressing issues related to convergence speed and parameter design. This approach simultaneously enhances the accuracy of estimating the SOC of lithium-ion batteries in energy storage stations. By simulating the immune mechanism of biological organisms, the algorithm achieves rapid convergence and global optimality, optimizing the weights and thresholds of the BP neural network. Additionally, the IGA creates a dynamic feedback effect during network training, accelerating the training process and improving the efficiency of network learning. The main novelties and contributions of this paper are as follows:

1. The mechanisms of temperature, current, and voltage impacts on SOC are revealed, laying the ground for determining the inputs of the proposed BP network. This can also provide guidelines for the similar future studies.
2. An improved BP neural network based on the IGA has been designed for estimating the SOC of lithium-ion batteries in energy storage stations. Compared with traditional BP neural networks, in this algorithm, the IGA is utilized to optimize the weights and thresholds of the BP neural network, effectively addressing the issues of convergence speed and parameter design associated with BP neural networks. This enhancement improves the accuracy of SOC estimation. Comparative experimental results prove the superiority of the proposed BP network.

The remainder of this article is organized as follows. In Section 2, the measurable quantities of lithium-ion batteries in energy storage stations are analyzed, including temperature, current, and voltage, with their relationship with SOC explained. In Section 3, the improved BP neural network based on the IGA will be introduced. In Section 4, experimental results will be presented to validate the proposed method. Finally, Section 5 serves as the conclusion section.

2. Mechanisms of temperature, current, and voltage impacts on SOC

Designing a BP neural network to detect the SOC of lithium-ion batteries necessitates explicitly defining both inputs and outputs. The SOC value itself constitutes the output. For inputs, it is essential to select variables that have a direct relationship with SOC. In the context of energy storage stations, temperature, current, and voltage are quantities that can be measured directly. This section delves into the underlying mechanisms linking these quantities to SOC, demonstrating their suitability as inputs for the neural network proposed in this study.

2.1. Mechanism of temperature impacts on SOC

a) Impact of temperature on battery internal resistance

The influence of temperature on batteries is complex and variable, making it challenging to track effectively. Temperature affects the battery's internal resistance, capacity, and open-circuit

voltage. When the temperature is too high, rapid chemical reactions within the battery can cause permanent damage to the internal materials, leading to a decrease in battery capacity [36]. Conversely, at low temperatures, the activity of the battery's internal materials is significantly reduced. Lithium ions cannot move normally through the separator, preventing the formation of electric current due to the lack of electron movement in the external circuit, thereby influencing the internal resistance.

Analyzing the relationship between lithium-ion battery internal resistance and temperature is essential for exploring the basic principles of internal reactions in lithium-ion batteries. Lithium-ion battery internal resistance is influenced by temperature and battery aging. To explore the impact of internal resistance and temperature, experiments are conducted with the same battery under different temperatures without involving multiple discharge cycles, to ensure the battery's aging level remains constant. The main reason for internal resistance in lithium-ion batteries is the obstruction faced by electrons moving between anodes and cathodes and the transfer of lithium ions between anodes and cathodes. The curve of lithium-ion battery internal resistance changes under different temperatures is shown in Fig. 2(a). The results are independently obtained from the battery pack given in Section 4. A programmable temperature control chamber HG-T-P-80J is utilized to adjust the ambient temperature surrounding the battery. By employing the DC resistance measurement method, the battery's internal resistance is tested under various temperature conditions. It can be noted that temperature significantly affects battery internal resistance, increasing as the temperature decreases. The basic principle is that lowering the temperature reduces the detachment and intercalation of lithium ions at the anodes and cathodes, slowing down the internal chemical reactions of the battery. This slows down electron movement, resulting in a rise in the internal resistance.

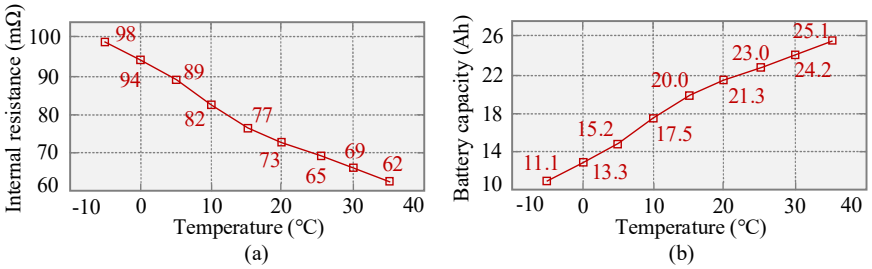

Fig. 2. Mechanism of temperature impacts on SOC: lithium-ion battery internal resistance under different temperatures (a); lithium-ion battery capacity under different temperatures (b)

b) Relationship between temperature and capacity

The rated capacity of lithium batteries varies with temperature. The activity of lithium ions increases with temperature, accelerating their movement and enhancing the anode and cathode materials' ability to accommodate lithium ions, thereby reducing resistance [37]. Higher temperatures increase the activity of anode and cathode materials, speeding up the detachment of lithium ions from the anode, moving quickly through the electrolyte to the cathode, and increasing the quantity of absorbed lithium ions, which boosts the lithium battery's capacity. During discharge, the speed at which lithium ions detach from the cathode increases, quickly accumulating at the anode, increasing external circuit current, balancing the internal charge, and thus increasing the

battery's capacity. The opposite occurs at lower temperatures. Temperature has a non-negligible impact on the capacity of lithium-ion batteries, making it essential to consider temperature effects when estimating the SOC and energy state of lithium-ion batteries. The capacity characteristic of lithium-ion batteries in our lab considering temperature impact is shown in Fig. 2(b). It indicates that temperature is a critical factor affecting battery capacity, yet the relationship between temperature and capacity is not linear. As temperature approaches the lower limit of the battery's allowable range, a similar change in temperature results in a more significant change in capacity. Conversely, as temperature approaches the upper limit, the battery's capacity change is minimal or very slight. As temperature gradually increases, its impact on battery capacity diminishes. Based on the relationship between lithium-ion batteries and temperature, to maximize the battery's utilization rate and capacity, it should operate within an appropriate temperature range. At higher temperatures, maximizing the battery's charge storage capability is paramount.

Overall, under low-temperature conditions, the battery exhibits high internal resistance and low capacity, preventing it from storing the same amount of electricity as possible under high-temperature conditions, resulting in a lower initial SOC. During operation, due to faster energy consumption, SOC decreases more rapidly. Therefore, temperature is a significant factor affecting SOC.

2.2. Mechanism of charging/discharging current impacts on SOC

The magnitude of charging and discharging currents fundamentally affects how quickly lithium-ion batteries can charge and discharge, influencing SOC fluctuations. A high charging current can swiftly elevate the battery's SOC, but too high currents risk causing uneven lithium deposition, leading to the formation of lithium dendrites. This can negatively affect battery performance and safety. On the flip side, a high discharging current can rapidly decrease SOC but may also lead to battery overheating. Intuitively, this accelerates energy consumption, causing SOC to decline more rapidly.

Additionally, like temperature, the magnitude of charging and discharging currents affects the battery's internal resistance, which in turn impacts the SOC. Resistance, indicative of the internal conductive path's resistance, is determined mainly by the electrolyte and electrode materials' conductivity. High current conditions increase the concentration gradient of ions in the electrolyte, leading to heightened resistance. Polarization resistance is associated with the electrochemical reactions during charging and discharging, encompassing both activation and concentration polarization on the electrodes' surface. High charging and discharging currents can accelerate these electrochemical reactions, potentially increasing both activation polarization and concentration polarization, and thus, polarization resistance. Moreover, high currents can amplify heat generation within the battery, influencing its temperature and, consequently, its internal resistance. Typically, a rise in temperature enhances the electrolyte's conductivity, reducing resistance. However, excessively high temperatures may compromise the battery's internal structure, increasing interface impedance. Figure 3 illustrates the trend of changing charging resistance across various discharging rates at the temperature of 20°. The results are independently obtained from the battery pack given in Section 4 as well. During test, the battery's charge is first discharged to the required SOC level. Then, the current is adjusted by manipulating the load (using a sliding rheostat), and the internal resistance of the battery is tested through the DC resistance measurement method. The results highlight the significant impacts of the charging rate on battery internal resistance. Generally, internal resistance exhibits an upward trend with increasing charging rates.

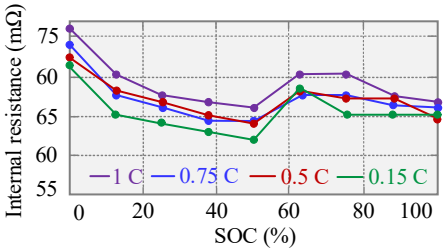

Fig. 3. Impact of current on battery internal resistance under different SOC

2.3. Relationship of voltage and SOC

The voltage of a battery has a close relationship with its SOC, a relationship that forms the basis for SOC estimation in battery management systems. Unlike the direct impacts of temperature and current, voltage serves as a fundamental characteristic of the battery. Its variations reflect changes in the battery's internal chemical reactions and charge state. Although changes in voltage do not directly alter the SOC value, voltage plays a crucial role in characterizing the battery's state and is instrumental in SOC estimation.

The relationship between battery voltage and SOC typically exhibits nonlinear characteristics, reflecting the battery's chemical properties and charge distribution at various SOC levels. As the SOC gradually decreases during the discharge process, the battery voltage also decreases; conversely, during charging, the battery voltage increases as the SOC rises. This trend may vary in slope at different charging and discharging stages, determined by the electrochemical properties of the battery's internal materials and the battery design itself. Given the clear relationship between battery voltage and SOC, voltage is often used as an intuitive method for estimating SOC. Although the accuracy of this method can be influenced by multiple factors, such as battery temperature and charging/discharging currents, a reasonable SOC estimate can still be obtained from the battery voltage under certain conditions. To enhance estimation accuracy, integrating additional methods such as neural networks can lead to more precise SOC predictions.

3. IGA-based BP neural network

This section introduces the design of an improved BP neural network based on the IGA, specifically tailored for estimating the SOC of lithium-ion batteries in energy storage stations. Initially, the basic structure of the BP neural network is established. Subsequently, the IGA is employed to enhance the parameter setting method of the BP neural network, thereby improving the estimation accuracy of the neural network.

3.1. Structure and mathematical model of BP neural network

The structure of the BP neural network for lithium-ion battery SOC estimation comprises three main parts: the input layer, the hidden layer, and the output layer, as shown in Fig. 4. The input layer receives three variables: temperature (T), current (I), and voltage (U), and the output is the estimated battery SOC value. For clarity, let's define the input vector as $\boldsymbol{X} = (x_1, x_2, x_3, x_4)$, where $x_1 = -1$, which represents the weight coefficient for each neuron in the hidden layer. As Section 2 thoroughly considers the variables that affect the accuracy of battery SOC estimation, and selects

battery voltage, temperature, and current as the input variables, that is, $x_2 = T$, $x_3 = I$, $x_4 = U$. The output vector of the hidden layer is $\boldsymbol{Y} = (y_1, y_2, \ldots, y_m)$, where m represents the number of neurons in the hidden layer. In theory, the more neurons in the hidden layer, the higher the estimation accuracy of the BP neural network. However, in practical applications, as the number of neurons in the hidden layer increases, the network's accuracy improves initially. But once the number of nodes in the hidden layer exceeds a certain threshold, the change in estimation accuracy becomes insignificant, and the estimation time actually increases, reducing the efficiency of the network. In this study, the hidden layer is designed with 20 neurons. The output layer vector is **Out** = (out), where out represents the estimated battery SOC value. Additionally, we define the desired output vector as $\boldsymbol{D} = (d)$. The weights corresponding to each neuron in the hidden layer and the input variables are represented by the matrix $\boldsymbol{V} = (v_{1i}, \ldots, v_{ki}, \ldots, v_{mi})$, where $i = 1, 2, 3, 4$. The weights between the output layer and the input variables are represented by the vector $\boldsymbol{W} = (w_j)$.

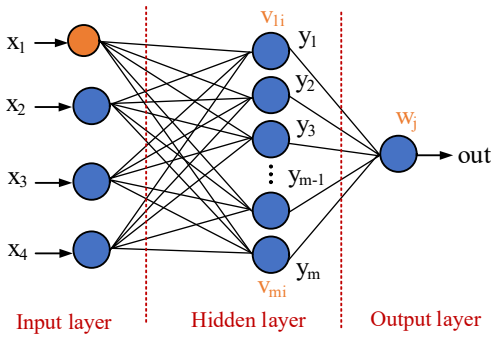

Fig. 4. Structure of the BP neural network for SOC estimation

The mathematical model of the output layer in a BP neural network is as follows:

$$\begin{cases} \text{out} = f(N_o) \\ N_o = \sum_{j=1}^{m} w_j y_j \end{cases}, \tag{1}$$

where $f(N_o)$ represents the activation function, $j = 1, 2, \ldots, m$, and m is the number of neurons in the hidden layer.

The mathematical model of the hidden layer is:

$$\begin{cases} y_k = f(N_{hk}) \\ N_{hk} = \sum_{i=1}^{4} v_{ki} x_i \end{cases}, \tag{2}$$

where $k = 1, 2, \ldots, m$. Activation functions are crucial for neural networks. According to reference [38], the sigmoid function exhibits several notable characteristics. Firstly, its smooth nature allows it to provide continuous gradient feedback during the learning process of the neural network, facilitating smooth adjustments to network parameters. Secondly, the S-shaped curve of the sigmoid function ensures effective gradient transmission within its activation range, particularly when the input values are close to 0, thereby promoting network learning. These advantages have

led to the widespread application of the sigmoid function in BP neural networks. In this study, the mathematical expression of the sigmoid function with respect to the variable N is as follows:

$$f(N) = \frac{1}{1 + e^{-N}}. \tag{3}$$

For the BP neural network depicted in Fig. 4, the mean squared error of its output is:

$$E = \frac{1}{2}(d - \text{out})^2. \tag{4}$$

By substituting (1) and (2) into (4), it can be obtained as:

$$E = \frac{1}{2}\left(d - f\left(\sum_{j=1}^{m} w_j f\left(\sum_{i=1}^{4} v_{ki} x_i\right)\right)\right)^2. \tag{5}$$

When adjusting the weight parameters of the neural network, they will be updated in the direction of the negative gradient, that is,

$$\begin{cases} \Delta w_j = -\eta \dfrac{\partial E}{\partial w_j} = -\eta \dfrac{\partial E}{\partial N_o} \dfrac{\partial N_o}{\partial w_j} = -\eta \dfrac{\partial E}{\partial N_o} y_j \\ \Delta v_{ki} = -\eta \dfrac{\partial E}{\partial v_{ki}} = -\eta \dfrac{\partial E}{\partial N_{hk}} \dfrac{\partial N_{hk}}{\partial v_{ki}} = -\eta \dfrac{\partial E}{\partial N_{hk}} x_i \end{cases}, \tag{6}$$

where Δw_j and Δv_{ki} represent the gradients of the output layer and the hidden layer, respectively. The negative sign indicates that the adjustment direction of the weights is in the opposite direction of the gradient. $\eta \in (0, 1)$ represents the learning rate of the neural network.

From the above formulas, it can be seen that the estimation error of the network can be expressed as a function related to the weights of the hidden layer and the input layer. Therefore, adjusting the weights of the network can change its estimation error. The principle of the BP neural network is based on this fact. Through continuous iterations of the network, the weights and thresholds are adjusted to ensure that the error meets the required accuracy.

3.2. BP neural network optimized by IGA

The IGA is a method developed by simulating the immune mechanism based on immunological theory. Its advantage lies in the ability to utilize the diversity of the immune system and maintain extreme values, thereby ensuring the diversity of the population. This overcomes the "premature convergence" phenomenon commonly encountered in general function optimization processes, ultimately ensuring the global nature of the optimization results. In the training process of BP neural networks, the IGA can be utilized to optimize key parameters, including the weight factors v_{ki} and w_j of each neuron, as well as the thresholds a and b of the hidden layer and output layer, which are used to determine whether the neural network operates with high accuracy. This chapter will design an improved BP neural network optimized by the IGA.

3.2.1. Development of IGA

The first step in the IGA is to simulate the biological immune mechanism for antigen recognition. In the context of the IGA, antigen recognition represents the objective function to be optimized, and the corresponding solution set is represented as antibodies. The IGA algorithm initially generates a number of antibodies in the initial population and evaluates the quality of the solution set through a fitness function. The fitness function, also known as affinity, indicates the closeness between the solution and the objective function. Then, new antibodies are produced in the population through crossover and mutation to update the population. Moreover, to enhance the diversity of the antibody population, mutation processing can be used in the population. The execution steps of the IGA are shown in Fig. 5. Below, the three key steps of the IGA are detailed: antigen recognition, affinity evaluation, and population update.

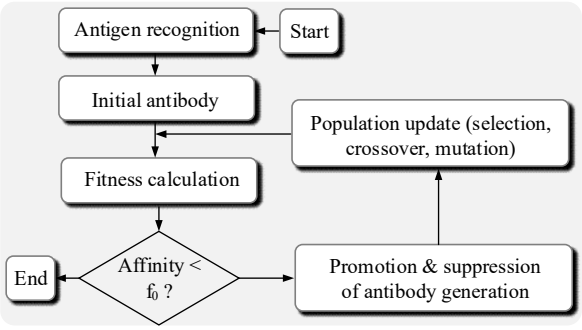

Fig. 5. Implementations of IGA

a) Antigen recognition

The first step of the IGA is to effectively identify the antigen. Simply put, this involves abstracting the problem of parameter optimization into a target function that needs to be solved. Subsequently, a certain number of random solution sets, corresponding to antibodies, are generated. During this process, the variables to be optimized need to be encoded. Denote $g_{i1} = (g_1, g_2, g_3, g_4) = (v_{ki}, w_j, a, b)$, where $i_1 = 1, 2, 3, 4$. The range of gi1 is defined as $[c_{i1}, d_{i1}]$, and the corresponding real-valued encoding can be represented as:

$$g_{i1} = a_{i1} + \lambda(d_{i1} - c_{i1}), \tag{7}$$

where λ is the regulation coefficient, and it ranges from 0 to 1.

b) Affinity evaluation

Before performing parameter optimization, it is essential to design an affinity function or fitness function to evaluate the performance of the antibodies, or the accuracy of the solutions. In this chapter, the affinity function used in the immune genetic algorithm is represented based on the accuracy of the BP neural network in estimating the SOC of lithium-ion batteries. The calculation formula is as follows:

$$f = \frac{|S_r - S_e|}{S_e} \times 100\%, \tag{8}$$

where S_r represents the true SOC value of the battery, while S_e is the SOC value estimated by the neural network. In practice, a constant value f_0 needs to be defined to judge whether f is less than it, which is the termination condition of the algorithms. Subsequently, a concentration function is

used to represent the similarity between each antibody in the population. During the continuous evolution and iteration of the population, it is usually necessary to promote and suppress the concentration of antibodies.

The calculation method for the concentration function of antibodies is as follows:

$$\begin{cases} c(x,y) = \dfrac{1}{1+s(x,y)} \times 100\% \\ s(x,y) = \dfrac{1}{n} \times \sum\limits_{i=1}^{n} |x_i - y_i| \end{cases}, \tag{9}$$

where c represents the concentration of antibodies, x and y refer to different antibodies, s is the similarity between different antibodies, and n is the number of antibodies.

For a given antibody, the probability p of being selected under the influence of both concentration and affinity is calculated as follows:

$$p = \frac{f \times e^{-\beta c}}{\sum\limits_{i=1}^{n} f \times e^{-\beta c}}, \tag{10}$$

where β is a regulating parameter.

c) Population update

Population update involves two processes: crossover and mutation, of which block diagrams are shown in Fig. 6. Crossover operation refers to the selection of two individuals from the population, followed by the exchange of randomly selected one or multiple chromosome positions between their different chromosomes. This process aims to generate more superior individuals.

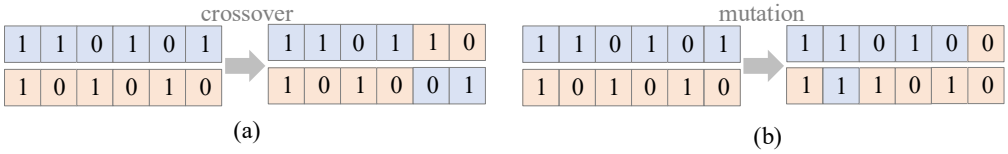

Fig. 6. Mechanisms of crossover and mutation: cross (a); mutation (b)

Randomly select two antibodies x and y from the population as the antibodies to be crossed and exchange parts of the antibody strings, performing a crossover operation between the two selected antibodies, which can be described as:

$$\begin{cases} x' = (1-r)x + r \cdot y \\ y' = (1-r)y + r \cdot x \end{cases}, \tag{11}$$

where x' and y' are the crossover variables, r is a random variable, ranging from 0 to 1. It needs to be mentioned that one selected antibody undergoes mutation at a fixed probability p_m. Taking x' as an example, its mutation can be described as:

$$x'' = \begin{cases} x' + (b' - x')p_m & r > 0.5 \\ x' + (x' - a')p_m & r \le 0.5 \end{cases}, \tag{12}$$

where x'' is the mutation variable, a' and b' are the lower and upper bounds, respectively.

3.2.2. Implementation of BP neural network optimized by IGA

Before estimating the SOC of lithium-ion batteries using a BP neural network, it is necessary to first train the network and construct a neural network model that can be used for battery SOC estimation. This process involves optimizing the BP neural network using the IGA. The training process of the new BP neural network is mainly divided into eleven stages, and the details are shown in Table 1, and the flowchart of algorithms implementation steps is shown in Fig. 7.

Table 1. BP neural network training process optimized based on IGA

Stages	Operations	Descriptions of the stages
1	Network initialization	Initialize the weights of each neuron in the BP neural network, v_{ki} and w_j, as well as the threshold of the hidden layer and the threshold of the output layer as a and b, respectively. In addition, the number of neurons in the input layer is 4, the number of neurons in the hidden layer (m) is 20, and the number of neurons in the output layer is 1.
2	Antigen recognition	Perform antigen recognition on the weight factors v_{ki}, w_j, and thresholds a, b that need to be optimized in the BP neural network. Additionally, initialize the IGA by setting the termination condition f_0, population size, maximum number of evolutions, crossover probability, and mutation probability.
3	Population initialization	Randomly generate a certain number of initial individuals to form the initial population.
4	Fitness evaluation of individuals:	Calculate the fitness value of each current individual, which represents the correlation between the solution set and the objective function.
5	Termination criteria for optimization algorithm	If the training requirements are met or the maximum number of evolution generations is reached, the loop is terminated. If the termination conditions are not met, the next step is executed.
6	Repeated optimization	Crossover, mutation, and other operations are performed according to the probabilities set for the initial network, and the population information is updated.
7	Updating population	The population reproduced through crossover and mutation operations is taken as the current population, and Sage 4 is continued until the termination conditions are met. The optimal solution set after searching for network parameters is recorded, and new network weights v_{ki}, w_j, and thresholds a, b are obtained.
8	Calculation of hidden layer output	Using (2), the output of the hidden layer $y_1, y_2, ..., y_m$ is calculated based on the input variables x_1, x_2, x_3, x_4 and the optimized connection weights v_{ki} between the input layer and the hidden layer.
9	Calculation of output layer	Using (1), the network output *out* is calculated based on the output of the hidden layer $y_1, y_2, ..., y_m$, the optimized connection weights w_j between the hidden layer and the output layer, and the threshold of the output layer.
10	Estimation error calculation of network	Using (4), based on the output result *out* and expected value d, calculate the estimation error E.
11	Termination criteria for network	Judge whether E satisfies the termination condition. If it is satisfied, stop the algorithms. Otherwise, move to Stage 4.

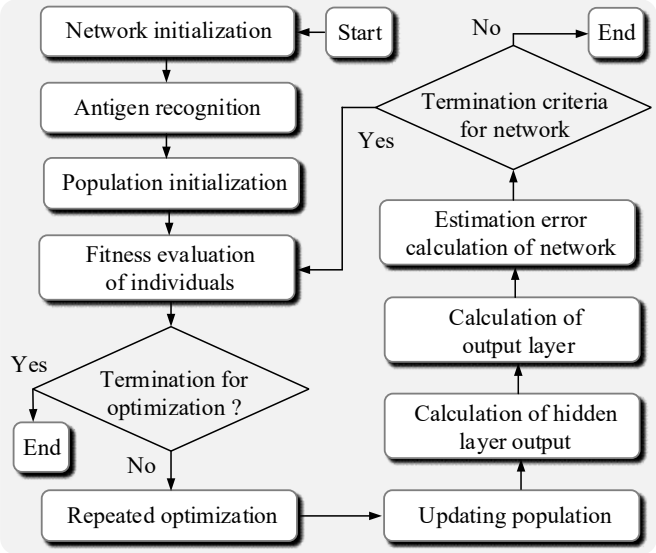

Fig. 7. Implementation steps of training algorithms

The overall structure of the proposed IGA-based BP neural network is depicted in Fig. 8.

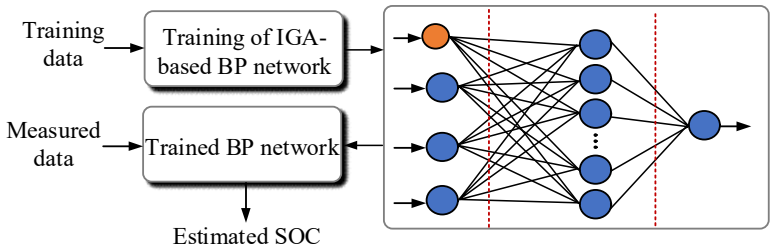

Fig. 8. Overall structure of proposed IGA-based BP neural network

4. Experimental verifications

To verify that the proposed BP neural network optimized by the IGA can effectively estimate the SOC of lithium-ion batteries, an experiment is conducted on a lithium-ion battery testing platform. The hardware of the test bench is shown in Fig. 9. The parameters of the lithium-ion battery are as follows. The rated capacity Q_{rated} is 20 Ah, open-circuit voltage E_{bat} is 60 V, and nominal internal resistance R_{bat} is 75 mΩ. Through a large number of tests, data for the training and validation of the BP neural network are collected. In the experiment, the battery current is controlled by adjusting the load resistance, and the voltage and current are measured by the voltage sensor LV25-P and the current sensor ACS712, respectively, and recorded on a host computer. For the sake of comparison, the SOC of the battery will also be measured and recorded by using the BTS-2002 battery tester. The battery is subjected to discharge experiments at 0.1 C, 0.4 C, 1 C, and 1.5 C under environmental temperatures of 15°C, 25°C, 35°C, and 50°C.

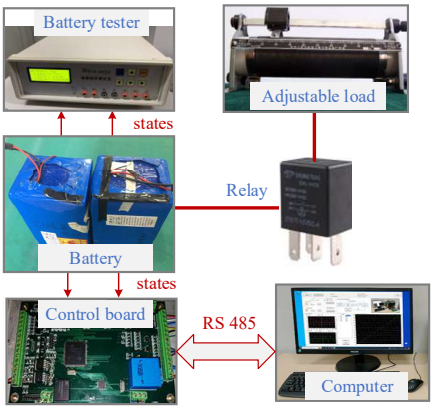

Fig. 9. Test bench used for verifying proposed SOC estimation algorithms

4.1. Construction of BP neural networks

Utilizing data obtained from testing under different temperatures and currents, both traditional BP neural networks and neural networks optimized with an IGA are trained using 10 000 samples. Figure 10 depicts the training convergence process of the two neural networks. When the output threshold is set to $a = b = 0.03$ (see Table 2), for both the traditional and the novel neural networks, the mean square error falls below the desired target after 1 033 and 864 iterations (decreasing by around 16.4%), respectively. This demonstrates that utilizing the IGA can achieve rapid convergence of the network.

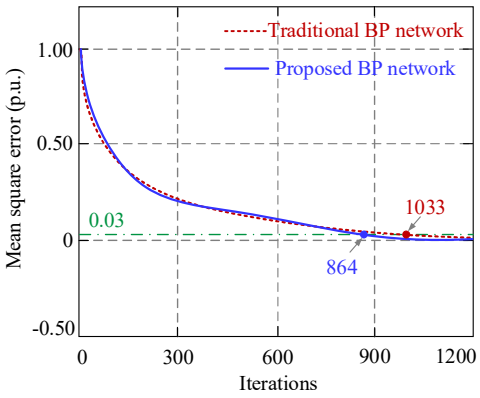

Fig. 10. Training convergence process of traditional and improved neural networks

Table 2. Parameters of BP neural networks

Parameters	Values	Parameters	Values
Number of neurons for input later	4	Termination condition f_0	3%
Number of neurons for hidden later m	20	Desired output d	Tested
Number of neurons for output later	1	Threshold of hidden layer b	0.03
Threshold of hidden layer a	0.03	Weight factors v_{ki} and w_j	0.65

To further demonstrate the superiority of the novel neural network in terms of training speed, the networks were trained using 30 000 and 50 000 data points, respectively. As shown in Table 3, when the mean square error is less than 0.03, the traditional BP neural network required 2 344 iterations and 4 889 seconds, respectively, for training. Comparatively, the new neural network required 1 840 iterations and 3 766 seconds, respectively, for training. These comparative results indicate that both the number of iterations and the training time for the new BP neural network are significantly reduced, demonstrating that the IGA accelerates the construction process of the BP neural network. When the number of training data increases to 50 000, a similar trend is observed.

Table 3. Comparative training processes of traditional and proposed BP neural networks

Algorithms	**Number of data**	**Iterations**	**Training time (s)**	**Mean square error (p.u.)**
Traditional BP network	10 000	1 033	1 885	0.029
	30 000	2 344	4 889	0.029
	50 000	4 765	8 453	0.03
Proposed BP network	10 000	864	1 320	0.027
	30 000	1 840	3 766	0.027
	50 000	3 522	6 866	0.028

4.2. SOC estimation results

By using the improved BP neural networks presented in Section 3, SOC estimation is carried out on batteries under 1 C discharge experiments at a temperature of 25°C, with the findings detailed in Fig. 11. Figure 11(a) illustrates the correlation between the voltage and the SOC of the battery, whereas Fig. 11(b) highlights the discrepancy between the estimated results and those

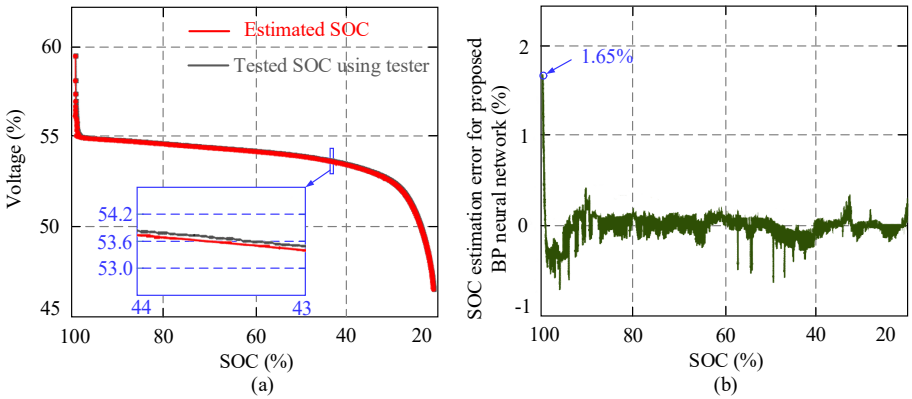

Fig. 11. Estimation results of proposed BP neural network: estimation and tested results (a); SOC estimation error between the estimated and tested results (b)

obtained through the BTS-2002 battery tester. Initially, across the entire testing framework, it's notable that the refined neural network approach exhibits superior estimation precision. When comparing with actual test outcomes, the peak estimation error registers at 1.65% when the SOC reaches 100%. Besides, the average error throughout the test period is around 0.35%. The improved BP neural network's ability to closely match the SOC values verified by the BTS-2002 tester indicates its potential for real-world applications. It suggests that with further refinement and calibration, such neural networks could become indispensable tools in the development of smart battery management systems that enhance the performance, safety, and longevity of battery packs.

For the sake of comparison, Fig. 12 presents the SOC estimation results of the traditional BP neural network. Figure 12 indicates that the traditional neural network also has high estimation accuracy. Compared to the results measured by the BTS-2002 battery tester, the estimation error is 1.96% when the SOC is at 100%, increasing by 18.8% compared to the proposed BP neural network. When the battery is at other SOC values, the estimation error is also slightly higher than that of the improved method, and the average value is about 0.68%. This demonstrates that the estimation error of the improved neural network is slightly lower than that of the traditional neural network, and its accuracy is improved, thereby enabling more accurate SOC estimation. This is consistent with the results shown in Table 3.

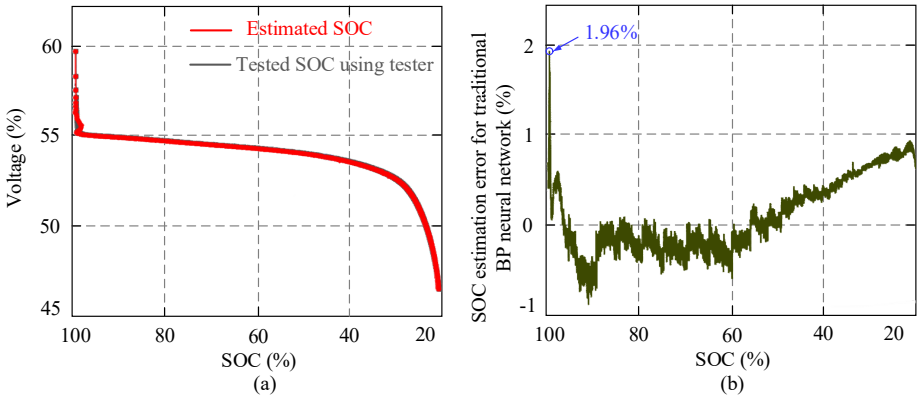

Fig. 12. Estimation results of traditional BP neural network: estimation and tested results (a); SOC estimation error between the estimated and tested results (b)

To further illustrate the accuracy of the new neural network, SOC estimation is performed on batteries subjected to 0.1 C, 0.4 C, 1 C, and 1.5 C discharge experiments at temperature of 35°C. The maximum SOC estimation errors during the testing process are shown in Table 4. For the traditional BP network, the estimation accuracy is 97.4% when the discharge current is 1 C, while it is 98.15% for the proposed BP network. This represents that the accuracy of the new strategy is around 1% higher than the traditional method. Besides, it can be seen that under any working condition, the estimation accuracy of the new neural network is slightly higher than that of the traditional neural network, which proves the effectiveness of the new method. Overall, the improved network's enhanced accuracy underlines the significance of integrating advanced neural network techniques for precise SOC estimations. This methodology not only reduces the training time but also minimizes SOC estimation errors, which represents the superiority of the proposed strategy.

Table 4. Maximum SOC estimation errors of traditional and improved BP neural networks

Current / Algorithms	0.1 C	0.4 C	1 C	1.5 C
Traditional BP network	4.6%	4.15%	2.6%	4.8%
Proposed BP network	3.5%	3.6%	1.85%	3.9%

5. Limitation and discussion

While the proposed method for optimizing BP neural networks using an immune genetic IGA shows significant improvements in the accuracy and efficiency of SOC estimation for lithium-ion batteries, several limitations and challenges need to be acknowledged.

The effectiveness of the proposed method heavily depends on the quality and quantity of the training data. In real-world applications, obtaining a comprehensive dataset that encompasses all possible operating conditions, such as varying temperatures, currents, and battery aging, can be challenging. Insufficient or unrepresentative data can lead to inaccuracies in SOC estimation. Although the IGA-optimized BP neural network converges faster than traditional BP neural networks, the computational complexity of implementing IGAs is still relatively high. This can be a limiting factor in scenarios where real-time SOC estimation is required, particularly in embedded systems with limited computational resources.

Furthermore, the study focuses specifically on lithium-ion batteries used in large-scale energy storage systems. Different battery chemistries (e.g., lead-acid, nickel-metal hydride) exhibit different behaviors and characteristics, meaning the proposed model might require significant adjustments or re-training to generalize across different battery types. Additionally, factors such as extreme environmental conditions, mechanical stress, and battery manufacturing inconsistencies can affect battery performance. While the proposed model accounts for temperature, current, and voltage, other environmental and operational factors could also impact SOC estimation accuracy.

Integrating the proposed method into existing battery management systems (BMS) on a large scale could be complex. Ensuring compatibility with various BMS architectures and protocols, as well as maintaining system stability and reliability, poses additional challenges. There is room for further optimization of the IGA parameters to balance convergence speed and computational efficiency. Advanced techniques such as adaptive genetic algorithms or hybrid methods combining IGAs with other optimization algorithms could be explored to enhance performance.

Future work should focus on the real-time implementation of the proposed method. Developing lightweight, efficient versions of the IGA-optimized BP neural network that can be deployed on embedded systems will be crucial for practical applications in BMS. To ensure the robustness of the proposed method, extensive cross-validation using diverse datasets is essential. This includes testing the model under various operating conditions and stress scenarios to evaluate its generalization capability and reliability.

The accurate SOC estimation provided by the proposed method can be integrated with predictive maintenance strategies. By monitoring battery health indicators and predicting potential failures, the method can contribute to extending battery life and reducing maintenance costs.

The adoption of advanced SOC estimation methods can have significant policy and economic implications. Accurate SOC estimation improves the efficiency and reliability of energy storage systems, supporting the broader integration of renewable energy sources into the grid. This, in turn, can contribute to achieving energy sustainability goals and reducing dependence on fossil fuels.

In conclusion, while the proposed IGA-optimized BP neural network method offers promising improvements in SOC estimation for lithium-ion batteries, addressing the identified limitations through further research and development will be critical for its successful real-world deployment.

6. Conclusions

This paper introduces a pioneering approach for estimating the SOC of lithium-ion batteries in energy storage power stations, utilizing an improved BP neural network optimized by an IGA. The research meticulously analyzes the effects of temperature, current, and voltage on the SOC, establishing a solid foundation for the neural network's input parameters. By employing the IGA to refine the BP neural network, the study overcomes common challenges associated with traditional BP networks, including slow convergence and complex parameterization, thereby improving the accuracy of SOC estimations and, consequently, the reliability of energy storage systems. The contributions of this paper are twofold. First, it reveals the mechanisms by which temperature, current, and voltage impact SOC, offering valuable insights for future research in battery management. Second, the design and implementation of an improved BP neural network optimized by the IGA represent a notable advancement in SOC estimation techniques. This approach not only addresses the limitations of traditional neural networks but also establishes a new standard for accuracy and operational efficiency in SOC estimation. Experimental results prove that the accuracy of the new method reaches 98.15%, which is about 1% higher than the traditional method. Overall, the proposed IGA-based BP network has enhanced accuracy and faster convergence in estimating the SOC of energy storage power stations, thereby being useful in practice.

Future work should focus on developing lightweight, efficient versions of the IGA-optimized BP neural network for real-time implementation in embedded systems. This includes extensive cross-validation using diverse datasets to ensure the model's robustness and generalization across various operating conditions. Additionally, integrating SOC estimation with predictive maintenance strategies can help extend battery life and reduce maintenance costs.

References

[1] Kumar R., Sahu B., Shiva C.K., Rajender B., *A control topology for frequency regulation capability in a grid integrated PV system*, Archives of Electrical Engineering, vol. 69, no. 2, pp. 389–401 (2020), DOI: 10.24425/aee.2020.133033.

[2] Kroposki B., *Integrating high levels of variable renewable energy into electric power systems*, Journal of Modern Power Systems and Clean Energy, vol. 5, no. 6, pp. 831–837 (2017), DOI: 10.1007/s40565-017-0339-3.

[3] https://www.reuters.com/sustainability/climate-energy/wind-solar-produce-over-third-global-power-by-2030-report-2023-07-13/, accessed July 2023.

[4] Jain H., Mather B., Jain A.K., Baldwin S.F., *Grid-supportive loads—A new approach to increasing renewable energy in power systems*, IEEE Transactions on Smart Grid, vol. 13, no. 4, pp. 2959–2972 (2022), DOI: 10.1109/TSG.2022.3153230.

[5] Jain V., Singh B., Seema Kewat, *A grid connected PV array and battery energy storage interfaced EV charging station*, IEEE Transactions on Transportation Electrification, vol. 9, no. 3, pp. 3723–3730 (2023), DOI: 10.1109/TTE.2023.3234994.

[6] Kaczorowska D., Rezmer J., Janik P., Sikorski T., *Smart control of energy storage system in residential photovoltaic systems for economic and technical efficiency*, Archives of Electrical Engineering, vol. 72, no. 1, pp. 81–102 (2023), DOI: 10.24425/aee.2023.143691.

[7] McKeon B.B., Furukawa J., Fenstermacher S., *Advanced lead–acid batteries and the development of grid-scale energy storage systems*, Proceedings of the IEEE, vol. 102, no. 6, pp. 951–963 (2014), DOI: 10.1109/JPROC.2014.2316823.

[8] Paliwal N.K., Singh A.K., Singh N.K., *Short-term optimal energy management in stand-alone microgrid with battery energy storage*, Archives of Electrical Engineering, vol. 67, no. 3, pp. 499–513 (2018), DOI: 10.24425/123659.

[9] Jafari S., Byun Y.C., *Prediction of the battery state using the digital twin framework based on the battery management system*, IEEE Access, vol. 10, pp. 124685–124696 (2022), DOI: 10.1109/ACCESS.2022.3225093.

[10] Li X., Wang S., *Energy management and operational control methods for grid battery energy storage systems*, CSEE Journal of Power and Energy Systems, vol. 7, no. 5, pp. 1026–1040 (2021), DOI: 10.17775/CSEEJPES.2019.00160.

[11] Seddjar A., Kerrouche K., Djamel E., Wang L., *Simulation of the proposed combined fuzzy logic control for maximum power point tracking and battery charge regulation used in CubeSat*, Archives of Electrical Engineering, vol. 69, no. 3, pp. 521–543 (2020), DOI: 10.24425/aee.2020.133916.

[12] Hallmann M., Wenge C., Komarnicki P., Balischewski S., *Methods for lithium-based battery energy storage SOC estimation. Part I: overview*, Archives of Electrical Engineering, vol. 71, no. 1, pp. 139–157 (2022), DOI: 10.24425/aee.2022.140202.

[13] Hallmann M., Wenge C., Komarnicki P., *Methods for lithium-based battery energy storage SOC estimation. Part II: application and accuracy*, Archives of Electrical Engineering, vol. 71, no. 2, pp. 311–323 (2022), DOI: 10.24425/aee.2022.140713.

[14] Zhou W., Zheng Y., Pan Z., Lu Q., *Review on the battery model and SOC estimation method*, Processes, vol. 9, no. 9, pp. 1685–1703 (2021), DOI: 10.3390/pr9091685.

[15] Zhang C., Xu X., Li Y., Huang J., Li C., Sun W., *Research on SOC estimation method for lithium-ion batteries based on neural network*, World Electric Vehicle Journal, vol. 14, no. 10, pp. 275–293 (2023), DOI: 10.3390/wevj14100275.

[16] Chang W.Y., *The state of charge estimating methods for battery: a review*, International Scholarly Research Notices, vol. 1, no. 953792, pp. 2356–7872 (2013), DOI: 10.1155/2013/953792.

[17] Hassini M., Redondo-Iglesias E., Venet P., *Lithium–ion battery data: from production to prediction*, Batteries, vol. 9, no. 7, pp. 385–404 (2023), DOI: 10.3390/batteries9070385.

[18] Zhang X., Hou J., Wang Z., Jiang Y., *Study of SOC estimation by the ampere-hour integral method with capacity correction based on LSTM*, Batteries, vol. 8, no. 10, pp. 170–190 (2022), DOI: 10.3390/batteries8100170.

[19] Giordano G., Klass V., Behm M., Lindbergh G., Sjöberg J., *Model-based lithium-ion battery resistance estimation from electric vehicle operating data*, IEEE Transactions on Vehicular Technology, vol. 67, no. 5, pp. 3720–3728 (2018), DOI: 10.1109/TVT.2018.2796723.

[20] Frivaldsky M., Simcak M., *Evaluation of the accuracy of the identified equivalent electrical circuit of LiPePO$_4$ battery through verified measurements*, Batteries, vol. 8, no. 5, pp. 38–56 (2022), DOI: 10.3390/batteries8050038.

[21] Jafari M., Malekjamshidi Z., Lu D.D.-C., Zhu J., *Development of a fuzzy-logic-based energy management system for a multiport multioperation mode residential smart microgrid*, IEEE Transactions on Power Electronics, vol. 34, no. 4, pp. 3283–3301 (2019), DOI: 10.1109/TPEL.2018.2850852.

[22] Hussein A.A., *Capacity fade estimation in electric vehicle Li-Ion batteries using artificial neutral networks*, IEEE Transactions on Industry Applications, vol. 51, no. 3, pp. 2321–2330 (2015), DOI: 10.1109/TIA.2014.2365152.

[23] Sun X., Chen Q., Zheng L., Yang J., *Joint estimation of state-of-health and state-of-charge for lithium-ion battery based on electrochemical model optimized by neural network*, IEEE Journal of Emerging and Selected Topics in Industrial Electronics, vol. 4, no. 1, pp. 168–177 (2023), DOI: 10.1109/JESTIE.2022.3148031.

[24] Azeroual M., Lamhamdi T., Moussaoui H.E., Markhi H.E., *Intelligent energy management system of a smart microgrid using multiagent systems*, Archives of Electrical Engineering, vol. 69, no. 1, pp. 23–38 (2020), DOI: 10.24425/aee.2020.131756.

[25] Fan X., Zhang W., Zhang C., Chen A., An F., *SOC estimation of Li-ion battery using convolutional neural network with U-Net architecture*, Energy, vol. 256, no. 1, pp. 1–9 (2022), DOI: 10.1016/j.energy.2022.124612.

[26] Zhang X., Liu X., Li J., *A novel method for battery SOC estimation based on slime mould algorithm optimizing neural network under the condition of low battery SOC value*, Electronics, vol. 12, no. 18, pp. 3924–3942 (2023), DOI:10.3390/electronics12183924.

[27] Guo Y., Zhao Z., Huang L., *SoC estimation of lithium battery based on improved BP neural network*, Energy Procedia, vol. 105, no. 1, pp. 4153–4158 (2017), DOI: 10.1016/j.egypro.2017.03.881.

[28] Liu X., Dai Y., *Energy storage battery SOC estimate based on improved BP neural network*, Journal of Physics: Conference Series, vol. 12, no. 42, pp. 1–6 (2021), DOI: 10.1088/1742-6596/2187/1/012042.

[29] Stefenon S.F., Seman L.O., Silva L.S. *et al.*, *Hypertuned temporal fusion transformer for multi-horizon time series forecasting of dam level in hydroelectric power plants*, International Journal of Electrical Power & Energy Systems, vol. 157, no. 109876, pp. 1–10 (2024), DOI: 10.1016/j.ijepes.2024.109876.

[30] Yi G., Zhuang X., Li Y., *Probabilistic state estimation in district heating grids using deep neural network*, Sustainable Energy, Grids and Networks, vol. 1, no. 1, pp. 1–10 (2024), DOI: 10.1016/j.segan.2024.101353.

[31] Lucas de Azevedo Takara *et al.*, *Deep reinforcement learning applied to a sparse-reward trading environment with intraday data*, Expert Systems with Applications, vol. 238, no. 121897 (2024), DOI: 10.1016/j.eswa.2023.121897.

[32] Grimm D., Tollner D., Kraus D. *et al.*, *A numerical verification method for multi-class feed-forward neural networks*, Epxert Systems with Applications, vol. 247, no. 123345 (2024), DOI: 10.1016/j.eswa.2024.123345.

[33] Mariani V.C. *et al.*, *Pressure prediction of a spark ignition single cylinder engine using optimized extreme learning machine models*, Applied Energy, vol. 249, no. 1, pp. 204–221 (2019), DOI: 10.1016/j.apenergy.2019.04.126.

[34] Wang Y., Lai C., *Multi-stage Neural Networks: Function Approximator of Machine Precision*, Journal of Computational Physics, vol. 504, no. 1, pp. 1–38 (2024), DOI:10.1016/j.jcp.2024.112865.

[35] Ribeirol G.T. *et al.*, *Novel hybrid model based on echo state neural network applied to the prediction of stock price return volatility*, Expert Systems with Applications, vol. 184, no. 1, pp. 1–17 (2021), DOI: 10.1016/j.eswa.2021.115490.

[36] Dikmen İ.C., Karadağ T., *Electrical method for battery chemical composition determination*, IEEE Access, vol. 10, pp. 6496–6504 (2022), DOI: 10.1109/ACCESS.2022.3143040.

[37] Nzereogu P.U. *et al*., *Anode materials for lithium-ion batteries: A review*, Applied Surface Science Advances, vol. 9, no. 100233, pp. 1–8 (2022), DOI: 10.1016/j.apsadv.2022.100233.

[38] Li Z., Zhang Y., Sui B., Xing Z., Wang Q., *FPGA implementation for the sigmoid with piecewise linear fitting method based on curvature analysis*, Electronics, vol. 11, no. 9, pp. 1365–1383 (2022), DOI: 10.3390/electronics11091365.